Electronic Detection of Lectins Using Carbohydrate-Functionalized Nanostructures: Graphene *versus* Carbon Nanotubes

Yanan Chen,[†] Harindra Vedala,[†] Gregg P. Kotchey,[†] Aymeric Audfray,[‡] Samy Cecioni,[‡,§] Anne Imberty,[‡] Sébastien Vidal,[§] and Alexander Star[†,*]

[†]Department of Chemistry, University of Pittsburgh, 219 Parkman Avenue, Pittsburgh, Pennsylvania 15260, United States, [‡]CERMAV—CNRS, affiliated with Université Joseph Fourier and ICMG, BP 53, 38041, Grenoble, France, and [§]Institut de Chimie et Biochimie Moléculaires et Supramoléculaires, Laboratoire de Chimie Organique 2—Glycochimie, UMR 5246, CNRS, Université Claude Bernard Lyon 1, 43 Boulevard du 11 Novembre 1918, F-69622, Villeurbanne, France

ABSTRACT

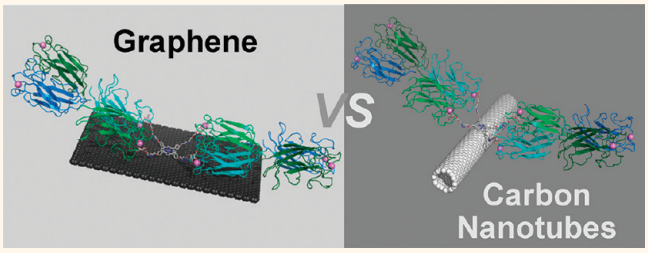

Here we investigated the interactions between lectins and carbohydrates using field-effect transistor (FET) devices comprised of chemically converted graphene (CCG) and single-walled carbon nanotubes (SWNTs). Pyrene- and porphyrin-based glycoconjugates were functionalized noncovalently on the surface of CCG-FET and SWNT-FET devices, which were then treated with 2 μM nonspecific and specific lectins. In particular, three different lectins (PA-IL, PA-IIL, and ConA) and three carbohydrate epitopes (galactose, fucose, and mannose) were tested. The responses of 36 different devices were compared and rationalized using computer-aided models of carbon nanostructure/glycoconjugate interactions. Glycoconjugate surface coverage in addition to one-dimensional structures of SWNTs resulted in optimal lectin detection. Additionally, lectin titration data of SWNT- and CCG-based biosensors were used to calculate lectin dissociation constants (K_d) and compare them to the values obtained from the isothermal titration microcalorimetry technique.

KEYWORDS: carbon nanotubes · graphene · carbohydrate · lectin · sensors

Because of their unique physical and chemical properties, single-walled carbon nanotubes (SWNTs) and more recently graphene have attracted considerable interest for the development of biosensors.[1−5] These carbon nanostructures are both just one atom thick, and their electronic properties are extremely sensitive to adsorption of chemical species on their surface. They have been successfully configured into field-effect transistor (FET) devices, which can be used for ultrasensitive detection of many chemical and biological molecules including proteins.[2,3]

Lectins are a class of nonimmune proteins that bind mono- and oligosaccharides reversibly and with high specificity.[6] Lectins have weak interaction with carbohydrates, in the form of glycoproteins, glycolipids, and glycans, in biological systems with dissociation constants (K_d) in the millimolar to micromolar range.[7−9] These interactions are involved in various biological processes, including cell—cell communication, pathogen binding, tumor cell metastasis, and immune responses. It is important to understand and mimic carbohydrate and bacterial lectin interactions as the foundation of pathogen detection and prevention of bacterial infection.[10−12]

Although carbon nanostructures have been functionalized using both covalent and noncovalent methods to induce specific lectin affinity,[13−17] the noncovalent functionalization route preserves physicochemical properties (*i.e.*, electrical conductivity) required for FET device operation. Utilizing this methodology, we have recently reported the noncovalent functionalization of SWNTs with glycosylated porphyrins for the detection of lectins with a SWNT-based FET device.[18]

In this work, we further investigated carbohydrate—lectin interactions with both SWNTs and chemically converted graphene (CCG), toward developing carbon nanostructure-based biosensors. In addition to glycosylated porphyrins, we also used pyrene-based glycoconjugates with both

* Address correspondence to astar@pitt.edu.

Received for review November 2, 2011 and accepted December 2, 2011.

Published online December 02, 2011
10.1021/nn2042384

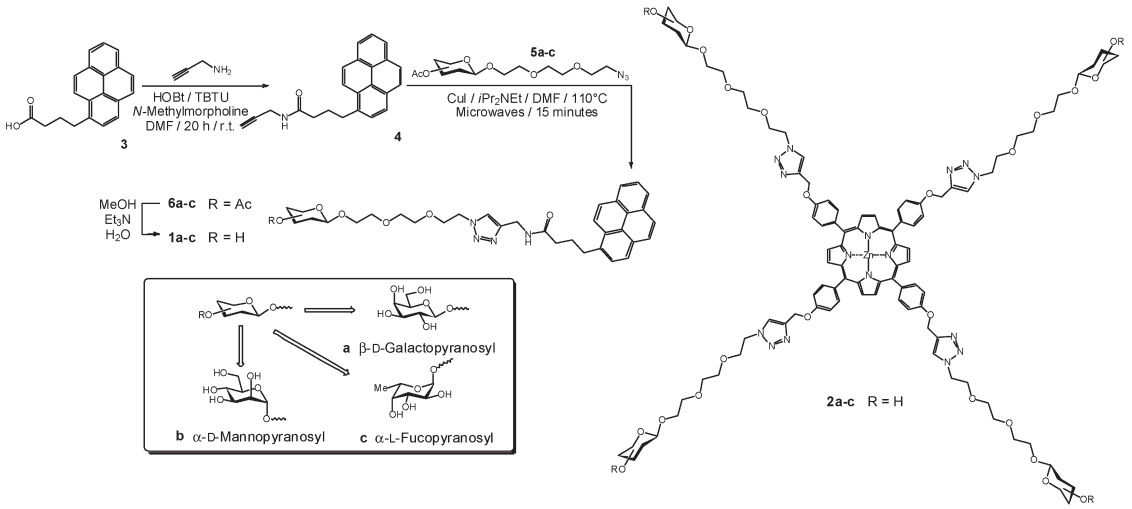

Scheme 1. Synthesis of pyrene-based glycoconjugates 1a, 1b, and 1c and general structure of porphyrin-based glycoconjugates 2a, 2b, and 2c.[18]

nanostructures. It should be mentioned here that among polynuclear aromatic compounds,[19] pyrene derivatives are recognized as highly effective labeling agents that are capable of forming $\pi-\pi$ stacking interactions with graphitic surfaces.[20−22] To date, pyrene−SWNT conjugate systems have been implemented with monosaccharides[15,17] and glycodendrimers[23] for lectin biosensing, drug delivery, or interfacing with living cells. Here we investigated SWNT-FET and CCG-FET devices noncovalently functionalized with pyrene- and porphyrin-based glycoconjugates carrying β-D-galactose, α-D-mannose, and α-L-fucose for nanoelectronic detection of lectins PA-IL, PA-IIL, and concanavalin A (ConA).

Lectins PA-IL and PA-IIL are produced in *Pseudomonas aeruginosa* together with other secondary metabolism virulence factors under quorum-sensing control and are involved in the infection process as demonstrated by the murine model.[24−26] *P. aeruginosa* bacteria are involved in cystic fibrosis lung infections, community infections such as otitis and pneumonia, and hospital-acquired infections.[27] PA-IL (13 kDa) is composed of four subunits of 121 amino acids and binds galactose plus its derivatives. PA-IIL (12 kDa) is composed of four subunits of 114 amino acids and binds fucose and other related monosaccharides. ConA (purified from jack-bean, *Canavalia ensiformis*, 25 kDa) lectin is a tetrameric lectin, which binds mannose and glucose. These three lectins require divalent cations for sugar-binding activity. Calcium ions mediate the binding of PA-IL and PA-IIL to their specific sugar moiety,[28,29] while calcium and manganese maintain the active conformation of a loop in ConA.[30]

RESULTS AND DISCUSSION

Our synthesis of pyrene-based glycoconjugates (**1a**, **1b**, **1c**) and porphyrin-based glycoconjugates (**2a**, **2b**, **2c**)[18] was achieved through 1,3-dipolar cycloaddition between alkynylated pyrene or porphyrin derivatives and azido-functionalized carbohydrates. The conjugation through Cu(I)-catalyzed alkyne−azide cycloaddition (CuAAC)[31−33] was preferred to the direct carboxylic acid-amine condensation methodology, which usually requires a significant excess of either reagent and the use of stoichiometric amounts of coupling reagents. In contrast, CuAAC requires only a catalytic amount of copper iodide and consumes a small excess of carbohydrate derivative (1.5 equivalents). The reaction of 1-pyrenebutyric acid **3** with propargyl amine afforded the corresponding amide **4**[34] in nearly quantitative yield. Subsequently CuAAC was performed between alkyne **4** and glycosylated azides **5a**−**c** under microwave activation[35−39] to obtain the acetylated pyrene-functionalized carbohydrate derivatives **6a**−**c**. The final deprotection step of acetyl groups was achieved by solvolysis to afford the desired hydroxylated pyrene glycoconjugates **1a**, **1b**, and **1c** in high yields (Scheme 1). The three glycoconjugates were fully characterized by 1D and 2D NMR and high-resolution mass spectrometry (see Supporting Information). This synthetic methodology has provided three glycosylated probes (β-D-galactose, α-D-mannose, α-L-fucose) ready to be immobilized on SWNTs or CCG for the detection of lectins with three different specificities (Table 1). The linker length was chosen on the basis of solubility,

TABLE 1. Glycoconjugates Used in This Study with Their Respective Specific and Control (Nonspecific) Lectins

	lectin	
glycoconjugate	specific	control
1a or **2a** (galactose)	PA-IL	ConA
1b or **2b** (mannose)	ConA	PA-IL
1c or **2c** (fucose)	PA-IIL	PA-IL

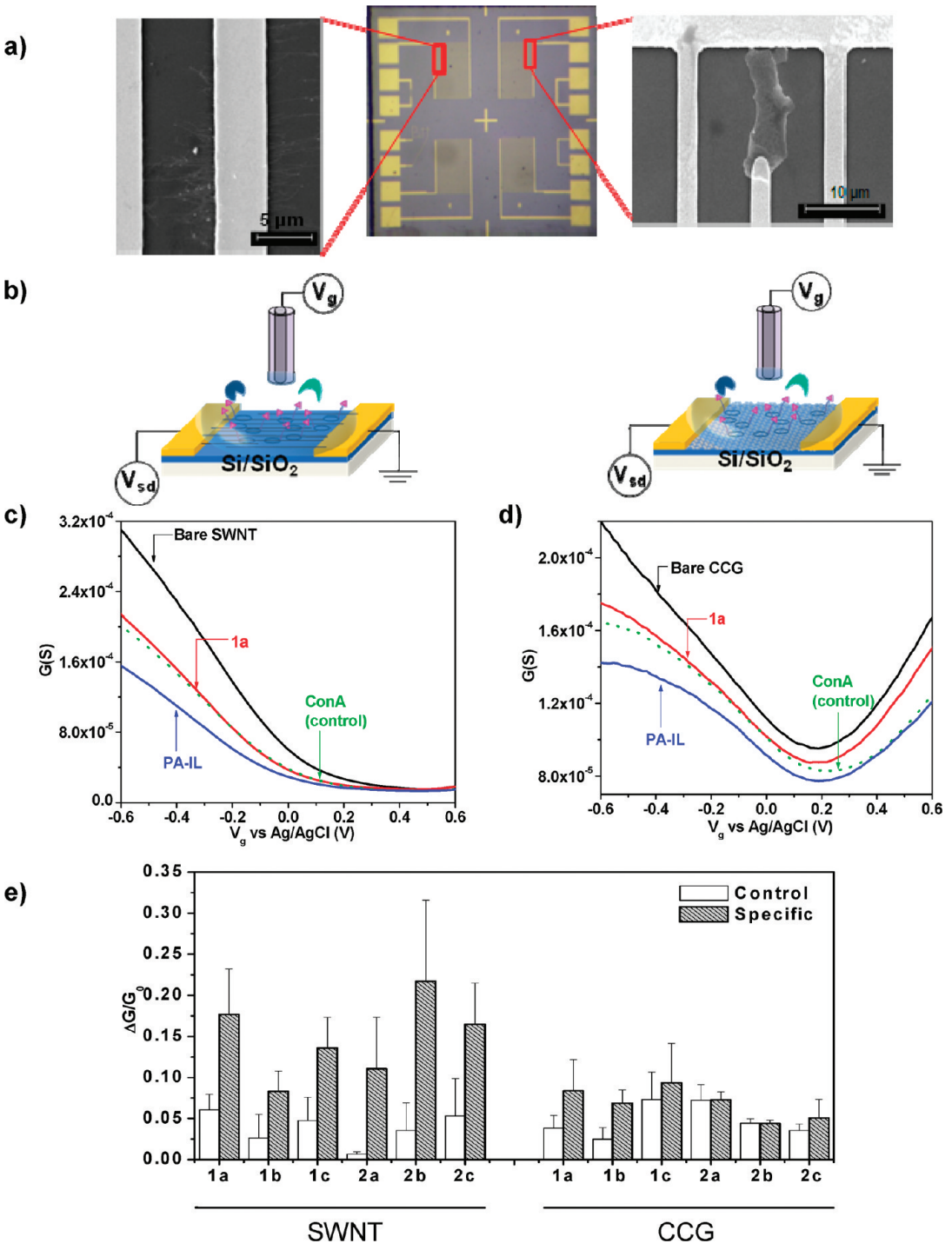

Figure 1. (a) Optical image of wirebonded Si chip with multiple photolithography patterned Au/Ti electrodes. Inset shows scanning electron microscopy (SEM) image of one set of the interdigitated electrodes (left, SWNT-FET; right, CCG-FET). (b) Schematic illustration of the liquid-gated FET configuration (left, SWNT-FET; right, CCG-FET). (c, d) Nanoelectronic detection of carbohydrate–lectin interactions: Conductance (*G*) *vs* gate voltage (V_g) of (c) bare SWNT-FET and (d) bare CCG-FET device after functionalization with β-D-galactose pyrene-based glycoconjugates (1a) and after attachment with 2 μM nonspecific (control) lectin ConA and 2 μM specific lectin PA-IL. (e) Comparison of the normalized responses ($V_g = -0.5$ V) to 2 μM control lectin and to 2 μM specific lectin for biosensors: SWNT+1a, 1b, 1c or 2a, 2b, 2c, CCG+1a, 1b, 1c or 2a, 2b, 2c. All measurements were performed in electrolyte-gated FET configuration in PBS (pH 7), Ag/AgCl reference electrode, with source–drain voltage of 50 mV. Lectin binding experiments were performed in the presence of 5 μM Ca^{2+}.

flexibility, and commercial availability of a desymmetrized triethyleneglycol.

Field-effect transistor devices comprising a CCG or SWNT network were fabricated by patterning interdigitated microelectrodes (source–drain spacing of 10 μm) on top of a 200 nm oxide layer on Si substrates using photolithography and e-beam evaporation of 30 nm of Ti and 100 nm of Au (Figure 1a).

Figure 1b depicts the schematic illustration of a liquid-gated FET configuration with either SWNTs or CCG as the conducting channel. CCG was prepared as described elsewhere.[40−42] CCG and SWNTs were deposited onto the device using an ac dielectrophoresis (DEP) method[43] (see Experimental Section). Carbon nanostructures were deposited between fingers of interdigitated microelectrodes, and the DEP method facilitated the alignment of SWNTs.[18]

To selectively detect lectins, SWNT-FET and CCG-FET devices were noncovalently functionalized with pyrene-based glycoconjugates. The noncovalent functionalization of carbon nanostructures with pyrene-based glycoconjugates was performed by incubating the Si chip with FET devices in a 20 μM solution of the glycoconjugates (in deionized water) for two hours followed by rinsing with deionized water three times. Upon interaction with pyrene-based glycoconjugates (**1a**−**c**), a decrease in the FET device conductance with a slight negative shift in gate voltage was observed (Figure 1c and d). The decrease in device conductance was attributed to electron donation from pyrene molecules to SWNTs or CCG conducting channels. The interactions were also studied by ultraviolet−visible−near-infrared (UV−vis−NIR) absorption spectroscopy, which indicated the attachment of the glycoconjugate to the carbon nanostructures (Figure S1).

After glycoconjugate functionalization, the FET devices were treated with nonspecific lectin (control) and then with specific binding lectins (both 2 μM lectins in PBS with 5 μM Ca^{2+}). Calcium ions were added to mediate the binding of lectins to their specific sugar moiety.[28−30] As presented in Figure 1c, SWNT-FET device functionalized with pyrene-glycoconjugate **1a** was treated with 2 μM nonspecific (ConA) and specific (PA-IL) lectins (in PBS with 5 μM Ca^{2+}). Upon treatment with nonspecific lectin, the transfer characteristics of the device remained unaffected. A decrease in device conductance was observed after treatment with specific lectin, which indicated selective interaction between the lectin and glycoconjugate. The same experiment with α-D-mannose and α-L-fucose pyrene-based glycoconjugates **1b** and **1c** also demonstrated a similar trend in response and selectivity (Figure S2).

To compare the CCG- and SWNT-FET devices for lectin detection, similar experiments were performed on pyrene glycoconjugates **1a**−**c** functionalized CCG-FET devices as well. Figure 1d shows the response of the **1a**-functionalized CCG-FET devices to various lectins. Compared to p-type SWNT-FET devices, CCG-FET had an ambipolar transfer characteristic and demonstrated different lectin responses at negative and positive gate voltages (p-type and n-type regions). To be consistent with the SWNT data, we compared the response in the p-type region only. Upon incubation with nonspecific lectin (ConA), there was a small decrease in conductance at negative gate voltages, while the decrease in the positive voltage region was larger. When treated with the galactose-specific lectin (PA-IL), a decrease was observed primarily at the negative gate voltages: Incidentally, the maximum selectivity for the CCG-FET devices was observed at the p-type region. The same experiments with α-D-mannose and α-L-fucose pyrene-based glycoconjugates **1b** and **1c** showed a similar response to the CCG/**1a** configuration (Figure S3). As an additional control, when bare CCG-FET devices were exposed to ConA, the device conductance decreased due to the nonspecific adsorption (Figure S4).

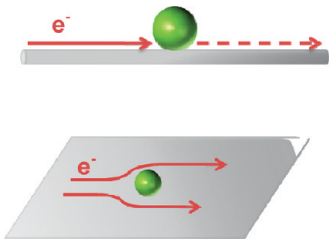

Scheme 2. Schematic illustration of lectin adsorption effects on an individual SWNT *versus* a single CCG flake.

Figure 1e summarizes the responses of all tested SWNT and CCG biodetectors to specific and nonspecific lectins (**1b**, **1c**, **2a**, **2b**, and **2c** data presented in Supporting Information). In all cases, we plotted the responses at negative gate voltages (V_g = −0.5 V), which allowed direct comparison between the two types of devices. For pyrene-based receptor molecules, SWNT-FET devices demonstrated a larger response and better selectivity for lectin detection than CCG. This may be attributed to the greater sensitivity to lectin adsorption on the transport properties of 1D SWNTs than 2D CCG.[44,45] We also compared the performance of SWNT-porphyrin and CCG-porphyrin (**2a**, **2b**, **2c**) biodetectors, and again SWNT-FET devices showed higher selectivity and response. Although glycoconjugates can have different interactions with either SWNTs or CCG, 1D systems should be generally more sensitive to the lectin binding (Scheme 2). Because lectin molecules have a size comparable to the diameter of SWNTs, even one molecule can effectively alter the electrical conductivity of SWNTs compared to significantly larger CCG flakes.

Since the better response of SWNTs may also be due to carbohydrate accessibility, computational modeling was performed to further understand the interaction between glycoconjugates, carbon nanomaterials, and lectins. Figure 2 illustrates molecular models of the interactions between the different carbon nanomaterials associated with galactosylated glycoconjugates and PA-IL lectin. Semiconducting SWNTs were built with chiral indices m = 14 and n = 4 as described previously,[46] which resulted in nanotubes with a 1.3 nm diameter. As displayed in Figure 2a and b, the

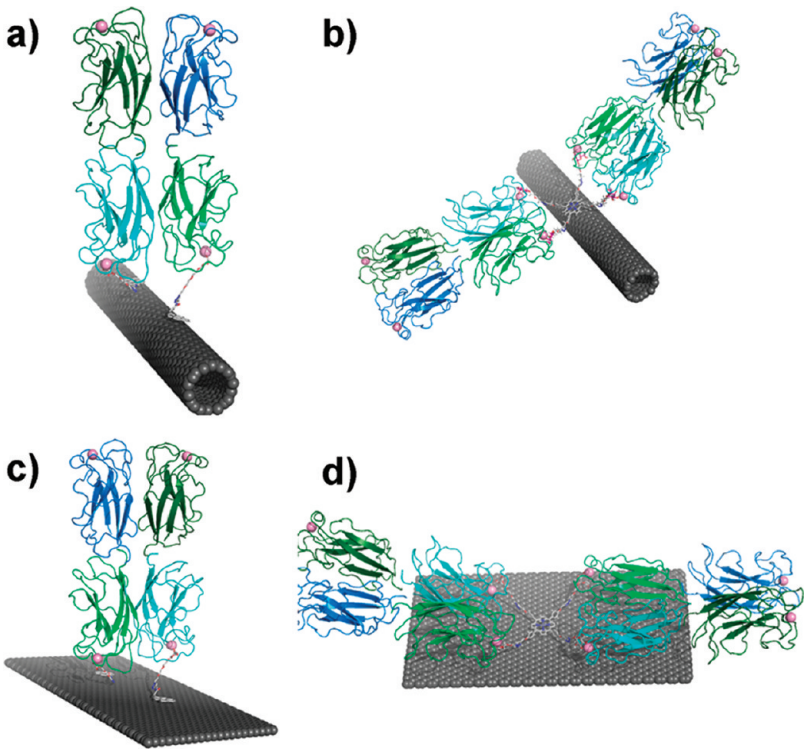

Figure 2. Computer-aided models of (a) SWNT/1a/PA-IL interaction, (b) SWNT/2a/PA-IL interaction, (c) CCG/ 1a/PA-IL interaction, and (d) CCG/2a/PA-IL interaction.

diameter of the SWNT is much smaller than the size of the lectin. The stacking of pyrene or porphyrin moieties of the glycoconjugates on the SWNT yielded galactose residues that are easily accessible for the lectins. Alternatively, stacking the same molecules on CCG resulted in galactose residues that were in close proximity to the carbon sheet and therefore less accessible for lectin binding. This is particularly true for porphyrin conjugates as displayed in Figure 2d. Therefore, it can be concluded that the SWNT system provides more flexibility for the sugar moieties to interact with lectin, leading to higher sensitivity than the CCG system.

To obtain evidence of the attachment of glycoconjugates onto the carbon nanostructure surfaces and the interaction between glycoconjugates and lectins, atomic force microscopy (AFM) imaging was performed at different stages of functionalization. The height of bare SWNTs was observed to be around 3−4 nm, indicating the presence of SWNT bundles (Figure 3a). After functionalization with α-D-mannose glycoconjugates **1b**, the total height increased to 5−7 nm (Figure 3b). After incubation with the nonspecific lectin PA-IL, the increase in height was 1−3 nm (Figure 3c). On the other hand, after exposing the glycoconjugate-functionalized SWNTs to the specific binding lectin (ConA for α-D-mannose), an increase in height of more than 10 nm was observed (Figure 3d). Bare CCG was observed to be 0.67 ± 0.15 nm in thickness (Figure 3e), which indicated the presence of a single-sheet structure. After functionalization with α-D-mannose glycoconjugates **1b**, the total height increased to 2.44 ± 0.35 nm (Figure 3f). When incubating with the nonspecific lectin PA-IL, the increase in height was around 1 nm (Figure 3g). After exposing the glycoconjugate-functionalized CCG to specific binding lectin (ConA for α-D-mannose), an increase in height to 8.25 ± 1.73 nm was observed (Figure 3h). The height measurements obtained by AFM were in good agreement with the literature values.[47] Typically, ConA was observed as a tetramer in solution at pH ≥ 7, and the molecular dimensions of the tetramer are 60 × 70 × 70 Å (Protein Data Bank, 1CN1), as determined from X-ray diffraction studies. As can be visualized from Figure 3d and h, SWNTs are covered continuously, while the binding sites are scattered randomly on the CCG surface. This indicates that the SWNT system provides more adsorption sites for lectins, which is consistent with the computer modeling studies. Additionally, the basal plane of CCG could contain oxygen functional groups (*i.e.*, epoxides and tertiary alcohols),[42] which could hinder the $\pi-\pi$ stacking of polynuclear aromatic compounds (glycoconjugates) and result in the lower lectin coverage. It should be mentioned here that the attachment of glycoconjugates to the surfaces of the nanostructure can effectively prevent the nonspecific binding of the lectin. For example, in Figure 3c and d, although PA-IL can adsorb nonspecificly onto the poly-L-lysine-decorated mica surface and form agglomerates, no evidence of nonspecific binding onto the **1b**-decorated surfaces of the

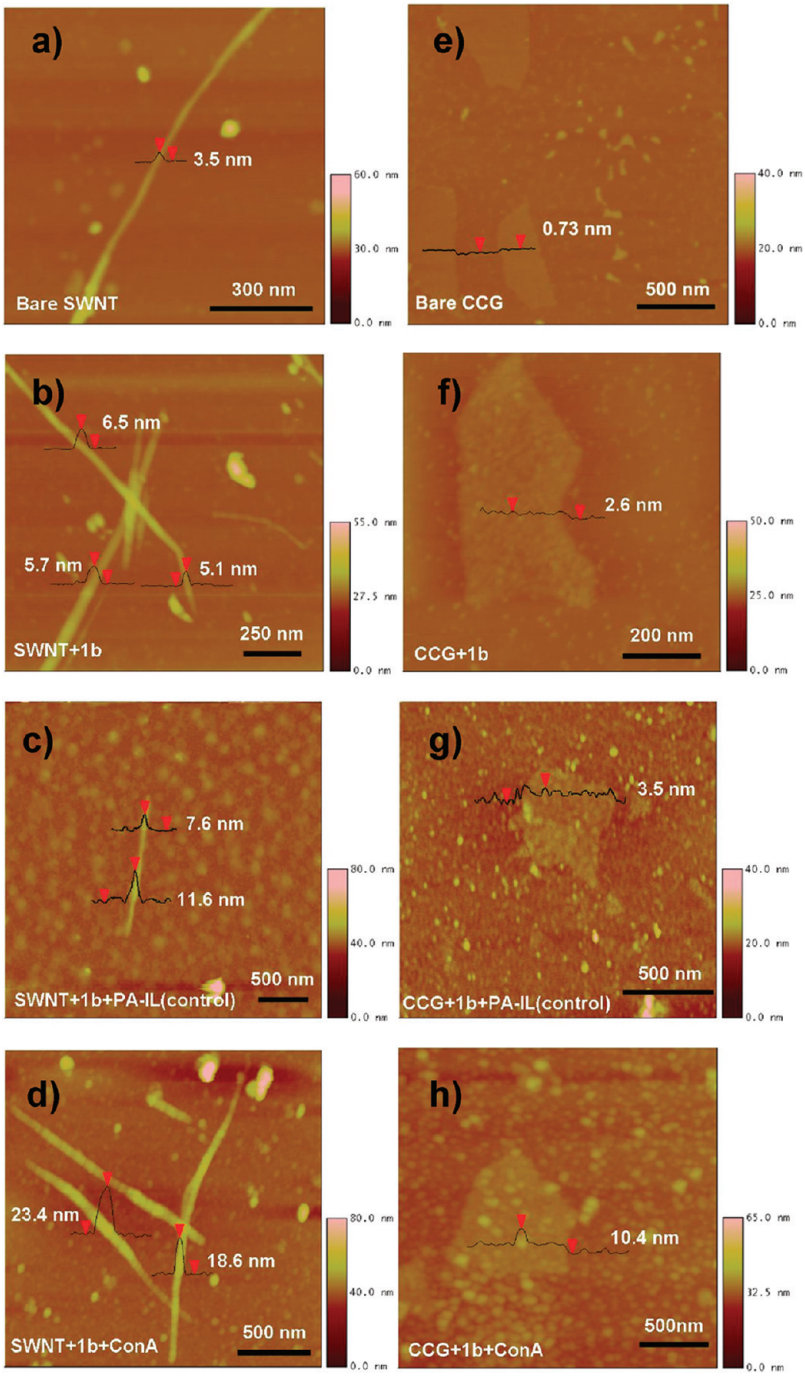

Figure 3. Atomic force microscope (AFM) images of (a) bare SWNTs, (b) SWNT functionalized with 1b, (c) after incubation with PA-IL (control), and (d) after ConA attachment; (e) bare CCG, (f) CCG functionalized with 1b, (g) after incubation with PA-IL (control), and (h) after ConA attachment. Lectin attachment was performed in the presence of 5 μM Ca^{2+}.

carbon nanostructure was observed. The high coverage of lectins on SWNTs in SWNT-FET devices was further illustrated by fluorescence microscopy. Figure 4 depicts the fluorescence image of an α-D-mannose-functionalized SWNT-FET device incubated with fluorescently labeled lectin ConA-Alexa488, which shows specific binding to α-D-mannose. SWNTs (aligned by DEP between fingers of interdigitated electrodes) clearly exhibit high fluorescence, indicating high coverage of ConA. Due to the fluorescence quenching effect of graphene,[48] no representative image for graphene flakes was obtained using fluorescence microscopy. The preferential lectin binding in addition to its pronounced effect on the electrical conductivity (Scheme 2) can explain the observed larger response and better selectivity of SWNT-FET devices.

Additionally, the sensitivity of SWNT-FET and CCG-FET devices was investigated by plotting the G *vs* V_g for the β-D-galactose-functionalized device (control

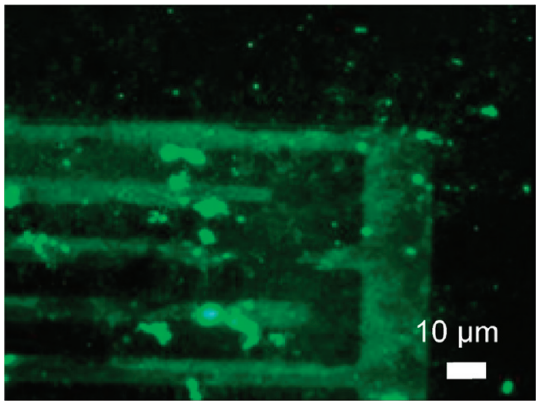

Figure 4. Fluorescence image of α-D-mannose glycoconjugates functionalized SWNT-FET device incubated with fluorescently labeled lectin ConA-Alexa488.

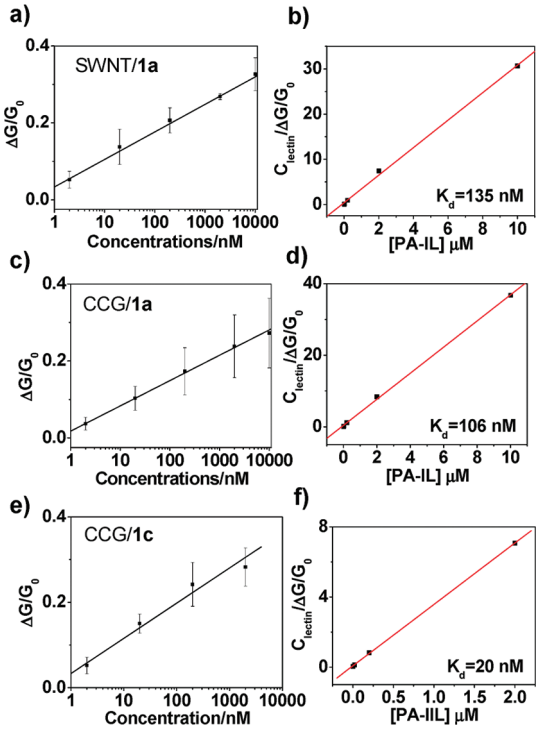

Figure 5. Biosensor calibration plot: normalized change in the device conductance (V_g = −0.5 V) *versus* PA-IL concentration of (a) SWNT-FET and (c) CCG-FET (data from three devices). Langmuir isotherm of (b) SWNT-FET data presented in panel (a), (d) for CCG-FET with their corresponding calculated lectin dissociation constants (K_d). (e) Calibration plot and (f) Langmuir isotherm of CCG/1c and PA-IIL interaction, with calculated lectin dissociation constant K_d.

measurements with 10 μM ConA) for varying concentration (2 nM to 10 μM) of specific lectin PA-IL (Figure S6). Figure 5a, c, and e depicts the biosensor calibration plot derived from multiconcentration experiments (data from three devices) for SWNT/**1a**, CCG/**1a**, and CCG/**1c**, respectively. The detection ability of the devices was also tested in the mixed sample of specific and nonspecific lectins. The device showed a similar signal compared to the pure sample of specific lectin (Figure S7).

TABLE 2. Comparison of K_d Values Obtained by FET and ITC Methods

		FET		
glycoconjugate	lectin	SWNT	CCG	ITC
1a/2a	PA-IL	135 nM/147.7 nM	106 nM	100 μM[a]/133 nM
1c	PA-IIL		20 nM	50 nM[a]

[a] K_d value for the carbohydrate binding site.

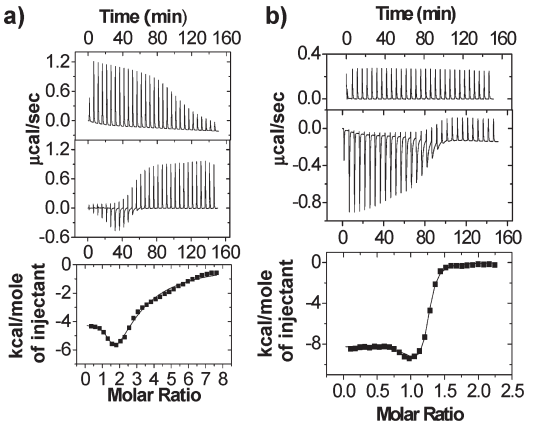

Figure 6. Titration of (a) PA-IL (0.05 mM) by compound 1a (1.7 mM) and (b) titration of PA-IIL (0.05 mM) by compound 1c (0.5 mM). Top: control (injection of glycoconjugate in buffer), middle: titration of lectin, bottom: integration of peaks with a fitting curve obtained from a two-site model.

To further understand the thermodynamics of the lectin−glycoconjugate interactions and to determine the dissociation constant (K_d) of the interaction, $C_{lectin}/(\Delta G/G_0)$ as a function of C_{lectin} were plotted, where C_{lectin} is the lectin concentration and $\Delta G/G_0$ is the relative change in conductance after lectin attachment (Figure 5).[49,50] A linear relationship was obtained, which indicated a Langmuir isotherm adsorption, and the **1a**/PA-IL K_d was calculated for SWNT-FET and CCG-FET as 135 and 106 nM, respectively. These values for galactose-based pyrene glycoconjugate interaction with PA-IL were similar to Kd (147.7 nM) calculated for porphyrin **2a** system (Figure S8). The **1c**/PA-IIL K_d was calculated for CCG-FET as 20 nM. These K_d values were compared with the values obtained by isothermal titration microcalorimetry (ITC) to explore the correlation between surface and solution binding (Table 2). The titration of the galactose and fucose pyrene-based conjugate (**1a** and **1c**) by their specific lectins (PA-IL and PA-IIL) followed by ITC (Figure 6a and b) indicated the occurrence of two binding events probably due to additional interaction of the pyrene aromatic group with a hydrophobic region on the lectins as previously evidenced for PA-IL.[51,52] Data treatment was performed using a two-site model (see Supporting Information S7), and only values for the carbohydrate binding sites are discussed below.

For PA-IL interacting with the galactose pyrene-based conjugate **1a**, the binding event in the galactose binding site had a dissociation constant of 0.1 mM, which was in agreement with data obtained on PA-IL/galactosides,[53] but is much weaker than the K_d of 106 and 135 nM obtained by FET measurement, when glycoconjugate **1a** is attached to CCG or SWNT, respectively (Figure 5b and d). This result was likely due to the chelating effect that has been evidenced for PA-IL binding to multivalent glycoconjugates with a 2 to 3 orders of magnitude increase in affinity when comparing multivalent ligands to monovalent ones.[37,53−55] Binding of PA-IL to glycoconjugates on surfaces or membranes has also been demonstrated to be more efficient than to monovalent compounds in solution.[56] The data obtained from the ITC experiment on porphyrin **2a**/PA-IL were in the range of 100 nM for both the solution and FET experiments, in agreement with the chelating effect since compound **2a** is tetravalent.

For PA-IIL interacting with fucose pyrene-based conjugate **1c**, a dissociation constant (K_d) of 50 nM was obtained for the fucose binding site, which was stronger than the one measured for methyl α-L-fucoside (430 nM).[57] The K_d value of **1c**/PA-IIL measured by FET experiment in Figure 5f was calculated as 20 nM and was consistent with the above-mentioned K_d value. No chelating effect has been observed for **1c**/PA-IIL binding.

ITC demonstrated that the carbohydrate moiety of the pyrene glycoconjugate is efficiently recognized by the corresponding lectin. The additional interaction of pyrene and the hydrophobic regions of the lectin occurs only in solution; therefore, this was not an issue in the FET experiment, where the pyrene moiety was stacked on the graphitic surface of either SWNT or CCG and not accessible for binding. Moreover, the K_d values obtained by ITC and FET are well correlated, which provided evidence of the effectiveness of carbon nanomaterial-based FET systems to detect carbohydrate−lectin interactions.

CONCLUSION

In conclusion, we have demonstrated the detection of interactions between glycoconjugates and bacterial lectins using SWNT-FET and CCG-FET devices functionalized with two receptor molecules, namely, porphyrin- and pyrene-based glycoconjugates. The interactions between lectins and glycoconjugates were transduced as conductance changes measured by SWNT-FET and CCG-FET devices. SWNT-FET showed larger response and better selectivity than CCG-FET, and we propose that this difference was the result of 1D and 2D structural differences between the two materials as well as more favorable lectin binding to sugar moieties attached to the SWNT surface. Because this nanoelectronic detection platform has the potential to be employed for the rapid identification of bacteria in samples consisting of water systems, soils, or human specimens, this technology upon further development may aid in preventing disease outbreaks and preserving public health.

EXPERIMENTAL SECTION

Materials and Methods. All reagents were procured commercially (highest purity available for reagent-grade compounds) and used without further purification. Solvents were distilled over CaH_2 (CH_2Cl_2) or Mg/I_2 (MeOH) or purchased as the highest purity available (DMF). Reactions were performed under an argon atmosphere. Reactions under microwave activation were performed on a Biotage Initiator system. Thin-layer chromatography (TLC) was carried out on aluminum sheets coated with silica gel 60 F_{254} (Merck). TLC plates were inspected by UV light ($\lambda = 254$ nm) and developed by treatment with a mixture of 10% H_2SO_4 in EtOH/H_2O (95:5 v/v) followed by heating. Silica gel column chromatography was performed with silica gel Si 60 (40−63 μm). NMR spectra were recorded at 293 K, unless otherwise stated, using a 300 MHz or a 400 MHz Brüker spectrometer. Chemical shifts are referenced relative to deuterated solvent residual peaks. The following abbreviations are used to explain the observed multiplicities: s, singlet; d, doublet; t, triplet; q, quadruplet; m, multiplet; and bs, broad singlet. Complete signal assignments were based on 1D and 2D NMR experiments (COSY, HSQC, and HMBC). High-resolution (HR-ESI-QToF) mass spectra were recorded by using a Brüker MicrOTOF-Q II XL spectrometer in the positive ionization mode. Optical rotations were measured using a Perkin-Elmer polarimeter, and values are given in 10^{-1} deg·cm^2·g^{-1}. The carbohydrate azido derivatives **5a**,[37,58] **5b**,[59] and **5c**[36,60] were previously described in the literature and prepared accordingly.

Single-walled carbon nanotubes were procured from Carbon Solutions Inc. Reduced graphene oxide, aka chemically converted graphene, was prepared as described elsewhere.[40−42] Briefly, graphite oxide was synthesized utilizing a modified Hummers' method on graphite flakes (Sigma Aldrich) that underwent a preoxidation step.[41] Graphite oxide (~0.125 wt %) was exfoliated to form graphene oxide *via* 30 min of ultrasonification followed by 30 min of centrifugation at 3400 rpm (rpm) to remove unexfoliated graphite oxide. Graphene oxide was then reduced to CCG with hydrazine hydrate (Sigma Aldrich) following the reported procedure.[40,42] Note that hydrazine is extremely flammable and toxic, and proper laboratory technique should be employed when handling this chemical.

PA-IL and PA-IIL lectins were produced in recombinant form, purified on an affinity column, extensively dialyzed, and lyophylized as described previously.[53,61] ConA (25 kDa) lectin was purchased from Sigma and was used without further purification.

Synthesis of the Pyrene-Glycoconjugates 1a, 1b, and 1c. *General Procedure for 1,3-Dipolar Cycloaddition (Method A).* The alkyne-functionalized pyrene derivative **4**, copper iodide, DIPEA, and carbohydrate azido derivatives **5a**−**c** in DMF were introduced in a Biotage Initiator 2−5 mL vial. The vial was flushed with argon, and the solution was sonicated for 30 s. The vial was sealed with a septum cap and heated at 110 °C for 30 min under microwave irradiation (solvent absorption level: high). After uncapping the vial, the crude mixture was evaporated and then purified by flash silica gel column chromatography to afford the desired acetylated pyrene glycoconjugates **6a**−**c**.

General Procedure for Deacetylation (Method B). The acetylated pyrene glycoconjugates **6a**−**c** were suspended in distilled MeOH, ultrapure water, and ultrapure triethylamine (10:1:1, v/v/v). The mixture was stirred under argon at room temperature for 1 to 3 days. Solvents were evaporated off, then coevaporated with toluene. The residue was dissolved in ultrapure water

(5 mL) and lyopholized to afford pure hydroxylated pyrene glycoconjugates **1a**, **1b**, and **1c**.

FET Measurements. Metal interdigitated devices (Au/Ti, 100 nm/30 nm) with an interelectrode spacing of 10 μm were patterned on a Si/SiO_2 substrate using conventional photolithography. Each chip (2 mm $\times$ 2 mm) containing six identical devices was then set into a 40-pin ceramic dual in-line package, wire-bonded using Au wire, and isolated by epoxying the device's inner cavity. SWNTs were deposited onto each interdigitated microelectrode pattern by ac dielectrophoresis (DEP) method from a suspension in *N*,*N*-dimethylformamide (DMF) (Agilent 33250A 80 MHz function/arbitrary waveform generator, with an applied ac frequency (10 MHz), bias voltage (8 V_{pp}), bias duration (60 s)).[18] CCG devices were prepared using the same DEP technique but with different parameters (ac frequency (300 kHz), bias voltage (10 V_{pp}), bias duration (120 s)).[43]

The electrical performance of each device was investigated using an electrolyte-gated FET device configuration. The conductance of the FET device was tuned using phosphate buffer solution (PBS) electrolyte as a highly effective gate. Two Keithley 2400 source meters were employed for FET measurements. A small fluid chamber (1 mL) was placed over the FET device to control the liquid environment using PBS at pH 7. A liquid gate potential (−0.75 to +0.75 V) with respect to the grounded drain electrode was applied using an Ag/AgCl (3 M KCl) reference electrode submerged in the gate electrolyte. The drain current of the device was measured at a constant source−drain voltage (50 mV). Transfer characteristics (conductance (*G*) *versus* gate voltage (V_g)) were measured.

Functionalization of the FET devices with each glycoconjugate was performed by incubating the chips in 20 μM of the glycoconjugates solution (in deionized water) for 2 h followed by rinsing three times with double-distilled water. After testing the transfer characteristics, the chips were incubated for 40 min in different concentrations of lectin solutions that were prepared in PBS with 5 μM $CaCl_2$ and subsequently washed three times with PBS solution. For each glycoconjugate-functionalized device, nonspecific lectins were tested first and subsequently washed away. The specific lectin was then added, and the final transfer characteristics were tested again in the configuration mentioned above.

Modeling Method. The SWNTs and graphene sheet were generated using Nanotube Modeler Software (JCrystalSoft, http://jcrystal.com). A semiconducting SWNT with a length of 10 nm and diameter of 1.3 nm was built using the chiral indices $m = 14$ and $n = 4$ as described previously.[46] A graphene sheet with dimension 5 $\times$ 10 nm^2 was built using the chiral indices $m = 20$ and $n = 0$. Zinc tetraphenyl porphyrin (ZnTPP) was built starting from the structure of Zn-protoporphyrin IX complexed with cytochrome *c* (PDB code 1I54). Pyrene and porphyrin galactosylated conjugates were built using the molecular editor in Sybyl software (Tripos, Inc., St Louis, MO, USA), and structures were minimized with the Tripos force field.[62] Galactosylated porphyrin **2a** was manually docked on the SWNT and sheet followed by energy minimization, while keeping the carbon structures fixed. Galactose linkers were adapted in order to generate distances between pairs of galactose residues of approximately 3 nm, compatible with binding to PA-IL adjacent sites. Final docking was performed by fitting galactose residues in proper locations or the binding sites as previously described.[37] A different procedure was used for the two galactosylated pyrenes **1a** that were first docked in two adjacent protein binding sites, before stacking the pyrene rings on the SWNT or graphene, with final energy minimization of the linker moiety.

Isothermal Titration Microcalorimetry. Recombinant lyophilized lectins were dissolved in buffer (20 mM Tris/HCl, 100 mM NaCl, 10 μM $CaCl_2$, pH 7.5) and degassed (see the Supporting Information for concentration details). Protein concentration was checked by measurement of optical density. Ligands were dissolved directly into the same buffer, degassed, and placed in the injection syringe. ITC was performed with a VP-ITC microcalorimeter (MicroCal Inc.). Lectins were placed into the 1.4478 mL sample cell at 25 °C. Each titration was performed with 10 μL injections of ligands every 300 s. Data were fitted with MicroCal Origin 7 software according to standard procedures. Two or three independent titrations were performed for each ligand tested.

Acknowledgment. This work was supported by NIEHS R01ES019304. Y.C. acknowledges a graduate student fellowship through Bayer MaterialScience. G.P.K. acknowledges an EPA STAR Graduate Fellowship, FP-91713801. The authors thank the Université Claude Bernard Lyon 1 and the CNRS for financial support. S.C. thanks the Région Rhône-Alpes (Cluster de Recherche Chimie) and the CNRS (Programme Interdisciplinaire: Chimie pour le Développement Durable) for additional funding. Dr. F. Albrieux, C. Duchamp, and N. Henriques are gratefully acknowledged for mass spectrometry analyses. Financial help is acknowledged from Vaincre la Mucoviscidose and GDR Pseudomonas. A.I. acknowledges funding from ANR Glycoasterix.

Supporting Information Available: Experimental details of UV−vis−NIR spectroscopy and AFM imaging, FET experiment of CCG and lectin interaction, UV−vis−NIR spectroscopy, AFM and fluorescence microscopy imaging, FET experiments of CCG and SWNT with pyrene-glycoconjugates functionalization, titration experiment of CCG and SWNTs with pyrene-glycoconjugates functionalization, FET experiments of CCG with porphyrin-glycoconjugates functionalization, Langmuir isotherm of CCG FET and SWNT FET data, experimental details for treatment of ITC data, and characterizations of glycoconjugates **1a**−**c** by 1D and 2D NMR and high-resolution mass spectrometry are available free of charge *via* the Internet at http://pubs.acs.org.

REFERENCES AND NOTES

1. Gustavo, A.; Jordi, R.; Ali, D.; Rius, F. Immediate Detection of Living Bacteria at Ultralow Concentrations Using a Carbon Nanotube Based Potentiometric Aptasensor. *Angew. Chem., Int. Ed.* **2009**, *48*, 7334–7337.
2. Star, A.; Gabriel, J.-C. P.; Bradley, K.; Grüner, G. Electronic Detection of Specific Protein Binding Using Nanotube FET Devices. *Nano Lett.* **2003**, *3*, 459–463.
3. Mao, S.; Lu, G.; Yu, K.; Bo, Z.; Chen, J. Specific Protein Detection Using Thermally Reduced Graphene Oxide Sheet Decorated with Gold Nanoparticle-Antibody Conjugates. *Adv. Mater.* **2010**, *22*, 3521–3526.
4. Zhang, B.; Cui, T. An Ultrasensitive and Low-Cost Graphene Sensor Based on Layer-by-Layer Nano Self-Assembly. *Appl. Phys. Lett.* **2011**, *98*, 073116.
5. Dong, X.; Shi, Y.; Huang, W.; Chen, P.; Li, L.-J. Electrical Detection of DNA Hybridization with Single-Base Specificity Using Transistors Based on CVD-Grown Graphene Sheets. *Adv. Mater.* **2010**, *22*, 1649–1653.
6. Lis, H.; Sharon, N. Lectins: Carbohydrate-Specific Proteins that Mediate Cellular Recognition. *Chem. Rev.* **1998**, *98*, 637–674.
7. Pieters, R. J. Maximising Multivalency Effects in Protein−Carbohydrate Interactions. *Org. Biomol. Chem.* **2009**, *7*, 2013–2025.
8. Dwek, R. A. Glycobiology: Toward Understanding the Function of Sugars. *Chem. Rev.* **1996**, *96*, 683–720.
9. Bertozzi, C. R.; Kiessling, L. L. Chemical Glycobiology. *Science* **2001**, *291*, 2357–2364.
10. Imberty, A.; Varrot, A. Microbial Recognition of Human Cell Surface Glycoconjugates. *Curr. Opin. Struct. Biol.* **2008**, *18*, 567–576.
11. Sharon, N. Carbohydrate−Lectin Interactions in Infectious Disease. *Adv. Exp. Med. Biol.* **1996**, *408*, 1–8.
12. Sharon, N. Carbohydrates as Future Anti-Adhesion Drugs for Infectious Diseases. *Biochim. Biophys. Acta* **2006**, *1760*, 527–537.
13. Hasegawa, T.; Fujisawa, T.; Numata, M.; Umeda, M.; Matsumoto, T.; Kimura, T.; Okumura, S.; Sakurai, K.; Shinkai, S. Single-Walled Carbon Nanotubes Acquire a Specific Lectin-Affinity through Supramolecular Wrapping with Lactose-Appended Schizophyllan. *Chem. Commun.* **2004**, 2150–2151.

14. Luo, P. G.; Wang, H.; Gu, L.; Lu, F.; Lin, Y.; Christensen, K. A.; Yang, S.-T.; Sun, Y.-P. Selective Interactions of Sugar-Functionalized Single-Walled Carbon Nanotubes with *Bacillus* Spores. *ACS Nano* **2009**, *3*, 3909–3916.
15. Assali, M.; Leal, M. P.; Fernandez, I.; Baati, R.; Mioskowski, C.; Khiar, N. Non-Covalent Functionalization of Carbon Nanotubes with Glycolipids: Glyconanomaterials with Specific Lectin-Affinity. *Soft Matter* **2009**, *5*, 948–950.
16. Khiar, N.; Leal, M. P.; Baati, R.; Ruhlmann, C.; Mioskowski, C.; Schultz, P.; Fernandez, I. Tailoring Carbon Nanotube Surfaces with Glyconanorings: New Bionanomaterials with Specific Lectin Affinity. *Chem. Commun.* **2009**, *27*, 4121–4123.
17. Sudibya, H. G.; Ma, J.; Dong, X.; Ng, S.; Li, L.; Liu, X.; Chen, P. Interfacing Glycosylated Carbon-Nanotube-Network Devices with Living Cells to Detect Dynamic Secretion of Biomolecules. *Angew. Chem., Int. Ed.* **2009**, *48*, 2723–2726.
18. Vedala, H.; Chen, Y.; Cecioni, S.; Imberty, A.; Vidal, S.; Star, A. Nanoelectronic Detection of Lectin-Carbohydrate Interactions Using Carbon Nanotubes. *Nano Lett.* **2011**, *11*, 170–175.
19. Assali, M.; Leal, M.; Fernández, I.; Romero-Gomez, P.; Baati, R.; Khiar, N. Improved Non-Covalent Biofunctionalization of Multi-walled Carbon Nanotubes Using Carbohydrates Amphiphiles with a Butterfly-like Polyaromatic Tail. *Nano Res.* **2010**, *3*, 764–778.
20. Holder, P. G.; Francis, M. B. Integration of a Self-Assembling Protein Scaffold with Water-Soluble Single-Walled Carbon Nanotubes. *Angew. Chem., Int. Ed.* **2007**, *46*, 4370–4373.
21. Prencipe, G.; Tabakman, S. M.; Welsher, K.; Liu, Z.; Goodwin, A. P.; Zhang, L.; Henry, J.; Dai, H. PEG Branched Polymer for Functionalization of Nanomaterials with Ultralong Blood Circulation. *J. Am. Chem. Soc.* **2009**, *131*, 4783–4787.
22. Simmons, T. J.; Bult, J.; Hashim, D. P.; Linhardt, R. J.; Ajayan, P. M. Noncovalent Functionalization as An Alternative to Oxidative Acid Treatment of Single Wall Carbon Nanotubes with Applications for Polymer Composites. *ACS Nano* **2009**, *3*, 865–870.
23. Wu, P.; Chen, X.; Hu, N.; Tam, U. C.; Blixt, O.; Zettl, A.; Bertozzi, C. R. Biocompatible Carbon Nanotubes Generated by Functionalization with Glycodendrimers. *Angew. Chem., Int. Ed.* **2008**, *47*, 5022–5025.
24. Imberty, A.; Wimmerová, M.; Mitchell, E. P.; Gilboa-Garber, N. Structures of the Lectins from *Pseudomonas Aeruginosa*: Insights into the Molecular Basis for Host Glycan Recognition. *Microbes Infect.* **2004**, *6*, 221–228.
25. Chemani, C.; Imberty, A.; de Bentzman, S.; Pierre, P.; Wimmerová, M.; Guery, B. P.; Faure, K. Role of LecA and LecB Lectins in *Pseudomonas Aeruginosa*-Induced Lung Injury and Effect of Carbohydrate Ligands. *Infect. Immun.* **2009**, *77*, 2065–2075.
26. Gilboa-Garber, N. *Pseudomonas aeruginosa* Lectins. *Methods Enzymol.* **1982**, *83*, 378–385.
27. Bodey, G. P.; Bolivar, R.; Fainstein, V.; Jadeja, L. Infections Caused by *Pseudomonas aeruginosa*. *Rev. Infect. Dis.* **1983**, *5*, 279–313.
28. Mitchell, E.; Houles, C.; Sudakevitz, D.; Wimmerova, M.; Gautier, C.; Pérez, S.; Wu, A. M.; Gilboa-Garber, N.; Imberty, A. Structural Basis for Oligosaccharide-Mediated Adhesion of *Pseudomonas aeruginosa* in the Lungs of Cystic Fibrosis Patients. *Nat. Struct. Biol.* **2002**, *9*, 918–921.
29. Cioci, G.; Mitchell, E. P.; Gautier, C.; Wimmerova, M.; Sudakevitz, D.; Pérez, S.; Gilboa-Garber, N.; Imberty, A. Structural Basis of Calcium and Galactose Recognition by the Lectin PA-IL of *Pseudomonas aeruginosa*. *FEBS Lett.* **2003**, *555*, 297–301.
30. Hardman, K. D.; Ainsworth, C. F. Structure of *Concanavalin* A at 2.4-Ang Resolution. *Biochemistry* **1972**, *11*, 4910–4919.
31. Meldal, M.; Tornoe, C. W. Cu-Catalyzed Azide-Alkyne Cycloaddition. *Chem. Rev.* **2008**, *108*, 2952–3015.
32. Rostovtsev, V. V.; Green, L. G.; Fokin, V. V.; Sharpless, K. B. A Stepwise Huisgen Cycloaddition Process: Copper(I)-Catalyzed Regioselective "Ligation" of Azides and Terminal Alkynes. *Angew. Chem., Int. Ed.* **2002**, *41*, 2596–2599.
33. Tornoe, C. W.; Christensen, C.; Meldal, M. Peptidotriazoles on Solid Phase: [1,2,3]-Triazoles by Regiospecific Copper-(I)-Catalyzed 1,3-Dipolar Cycloadditions of Terminal Alkynes to Azides. *J. Org. Chem.* **2002**, *67*, 3057–3064.
34. Ahlborn, C.; Siegmund, K.; Richert, C. Isostable DNA. *J. Am. Chem. Soc.* **2007**, *129*, 15218–15232.
35. Bouillon, C.; Meyer, A.; Vidal, S.; Jochum, A.; Chevolot, Y.; Cloarec, J.-P.; Praly, J.-P.; Vasseur, J.-J.; Morvan, F. Microwave Assisted "Click" Chemistry for the Synthesis of Multiple Labeled-Carbohydrate Oligonucleotides on Solid Support. *J. Org. Chem.* **2006**, *71*, 4700–4702.
36. Morvan, F.; Meyer, A.; Jochum, A.; Sabin, C.; Chevolot, Y.; Imberty, A.; Praly, J.-P.; Vasseur, J.-J.; Souteyrand, E.; Vidal, S. Fucosylated Pentaerythrityl Phosphodiester Oligomers (PePOs): Automated Synthesis of DNA-Based Glycoclusters and Binding to *Pseudomonas aeruginosa* Lectin (PA-IIL). *Bioconjugate Chem* **2007**, *18*, 1637–1643.
37. Cecioni, S.; Lalor, R.; Blanchard, B.; Praly, J.-P.; Imberty, A.; Matthews, S. E.; Vidal, S. Achieving High Affinity towards a Bacterial Lectin through Multivalent Topological Isomers of Calix[4]Arene Glycoconjugates. *Chem.—Eur. J.* **2009**, *15*, 13232–13240.
38. Moni, L.; Pourceau, G.; Zhang, J.; Meyer, A.; Vidal, S.; Souteyrand, E.; Dondoni, A.; Morvan, F.; Chevolot, Y.; Vasseur, J.-J.; *et al.* Design of Triazole-Tethered Glycoclusters Exhibiting Three Different Spatial Arangements and Comparative Study of Their Affinity for PA-IL And RCA 120 Using a DNA-Based Glycoraray. *ChemBioChem* **2009**, *10*, 1369–1378.
39. Cecioni, S.; Faure, S.; Darbost, U.; Bonnamour, I.; Parrot-Lopez, H.; Roy, O.; Taillefumier, C.; Wimmerová, M.; Praly, J.-P.; Imberty, A.; *et al.* Selectivity among Two Lectins: Probing the Effect of Topology, Multivalency and Flexibility of "Clicked" Multivalent Glycoclusters. *Chem.—Eur. J.* **2011**, *17*, 2146–2159.
40. Li, D.; Müller, M. B.; Gilje, S.; Kaner, R. B.; Wallace, G. G. Processable Aqueous Dispersions of Graphene Nanosheets. *Nat. Nanotechnol.* **2008**, *3*, 101–105.
41. Kovtyukhova, N. I.; Ollivier, P. J.; Martin, B. R.; Mallouk, T. E.; Chizhik, S. A.; Buzaneva, E. V.; Gorchinskiy, A. D. Layer-by-Layer Assembly of Ultrathin Composite Films from Micron-Sized Graphite Oxide Sheets and Polycations. *Chem. Mater.* **1999**, *11*, 771–778.
42. Kotchey, G. P.; Allen, B. L.; Vedala, H.; Yanamala, N.; Kapralov, A. A.; Tyurina, Y. Y.; Klein-Seetharaman, J.; Kagan, V. E.; Star, A. Enzymatic Oxidation of Graphene Oxide. *ACS Nano* **2011**, *5*, 2098–2108.
43. Vijayaraghavan, A.; Sciascia, C.; Dehm, S.; Lombardo, A.; Bonetti, A.; Ferrari, A. C.; Krupke, R. Dielectrophoretic Assembly of High-Density Arrays of Individual Graphene Devices for Rapid Screening. *ACS Nano* **2009**, *3*, 1729–1734.
44. Tang, Y.; Kotchey, G. P.; Vedala, H.; Star, A. Electrochemical Detection with Platinum Decorated Carbon Nanomaterials. *Electroanalysis* **2011**, *23*, 870–877.
45. Wanekaya, A.; Chen, W.; Myung, N.; Mulchandani, A. Nanowire-Based Electrochemical Biosensors. *Electroanalysis* **2006**, *18*, 533–550.
46. Allen, B. L.; Kotchey, G. P.; Chen, Y.; Yanamala, N. V. K.; Klein-Seetharaman, J.; Kagan, V. E.; Star, A. Mechanistic Investigations of Horseradish Peroxidase-Catalyzed Degradation of Single-Walled Carbon Nanotubes. *J. Am. Chem. Soc.* **2009**, *131*, 17194–17205.
47. Waner, M. J.; Gilchrist, M.; Schindler, M.; Dantus, M. Imaging the Molecular Dimensions and Oligomerization of Proteins at Liquid/Solid Interfaces. *J. Phys. Chem. B* **1998**, *102*, 1649–1657.
48. Loh, K. P.; Bao, Q.; Eda, G.; Chhowalla, M. Graphene Oxide as a Chemically Tunable Platform for Optical Applications. *Nat. Chem.* **2010**, *2*, 1015–1024.
49. Seo, J. H.; Kim, C. P.; Hwang, B. H.; Cha, H. J. A Functional Carbohydrate Chip Platform for Analysis of Carbohydrate-Protein Interaction. *Nanotechnology* **2010**, *21*, 215101.
50. Szunerits, S.; Niedziołka-Jonsson, J.; Boukherroub, R.; Woisel, P.; Baumann, J. S.; Siriwardena, A. Label-Free Detection of

Lectins on Carbohydrate-Modified Boron-Doped Diamond Surfaces. *Anal. Chem.* **2010**, *82*, 8203–8210.
51. Stoitsova, S. R.; Boteva, R. N.; Doyle, R. J. Binding of Hydrophobic Ligands by *Pseudomonas aeruginosa* PA-I Lectin. *Biochim. Biophys. Acta* **2003**, *1619*, 213–219.
52. Garber, N.; Guempel, U.; Belz, A.; Gilboa-Garber, N.; Doyle, R. J. On the Specificity of the D-Galactose-Binding Lectin (Pa-I) of *Pseudomonas Aeruginosa* and Its Strong Binding to Hydrophobic Derivatives of D-Galactose and Thiogalactose. *Biochim. Biophys. Acta* **1992**, *1116*, 331–333.
53. Blanchard, B.; Nurisso, A.; Hollville, E.; Tétaud, C.; Wiels, J.; Pokorna, M.; Wimmerova, M.; Varrot, A.; Imberty, A. Structural Basis of the Preferential Binding for Globo-Series Glycosphingolipids Displayed by *Pseudomonas aeruginosa* lectin I (PA-IL). *J. Mol. Biol.* **2008**, *383*, 837–853.
54. Kadam, R. U.; Bergmann, M.; Hurley, M.; Garg, D.; Cacciarini, M.; Swiderska, M. A.; Nativi, C.; Sattler, M.; Smyth, A. R.; Williams, P.; *et al*. A Glycopeptide Dendrimer Inhibitor of the Galactose Specific Lectin LecA and of Pseudomonas aeruginosa Biofilms. *Angew. Chem., Int. Ed.* **2011**, *50*, 10631–10635.
55. Chabre, Y. M.; Giguère, D.; Blanchard, B.; Rodrigue, J.; Rocheleau, S.; Neault, M.; Rauthu, S.; Papadopoulos, A.; Arnold, A. A.; Imberty, A.; *et al*. Combining Glycomimetic and Multivalent Strategies toward Designing Potent Bacterial Lectin Inhibitors. *Chem.—Eur. J.* **2011**, *17*, 6545–6562.
56. Sicard, D.; Cecioni, S.; Iazykov, M.; Chevolot, Y.; Matthews, S. E.; Praly, J.-P.; Souteyrand, E.; Imberty, A.; Vidal, S.; Phaner-Goutorbe, M. AFM Investigation of *Pseudomonas aeruginosa* Lectin Leca (PA-IL) Filaments Induced by Multivalent Glycoclusters. *Chem. Commun.* **2011**, 9483–9485.
57. Sabin, C.; Mitchell, E. P.; Pokorna, M.; Gautier, C.; Utille, J.-P.; Wimmerova, M.; Imberty, A. Binding of Different Monosaccharides by Lectin PA-IIL from *Pseudomonas aeruginosa*: Thermodynamics Data Correlated with X-Ray Structures. *FEBS Lett.* **2006**, *580*, 982–987.
58. Szurmai, Z.; Szabo, L.; Liptak, A. Diethylene and Triethylene Glycol Spacers for the Preparation of Neoglycoproteins. *Acta Chim. Hung.* **1989**, *126*, 256–269.
59. Li, J.; Zacharek, S.; Chen, X.; Wang, J.; Zhang, W.; Janczuk, A.; Wang, P. G. Bacteria Targeted by Human Natural Antibodies Using Alpha-Gal Conjugated Receptor-Specific Glycopolymers. *Bioorg. Med. Chem* **1999**, *7*, 1549–1558.
60. Sanki, A.; Mahal, L. A One-Step Synthesis of Azide-Tagged Carbohydrates: Versatile Intermediates for Glycotechnology. *Synlett* **2006**, 455–459.
61. Mitchell, E. P.; Sabin, C.; Snajdrova, L.; Budova, M.; Perret, S.; Gautier, C.; Hofr, C.; Gilboa-Garber, N.; Koča, J.; Wimmerová, M.; *et al*. High Affinity Fucose Binding of *Pseudomonas aeruginosa* Lectin PA-IIL: 1.0 Å Resolution Crystal Structure of the Complex Combined with Thermodynamics and Computational Chemistry Approaches. *Proteins* **2005**, *58*, 735–748.
62. Clark, M.; Cramer, R. D., III; van Opdenbosch, N Validation of the General Purpose Tripos 5.2 Force Field. *J. Comput. Chem.* **1989**, *10*, 982–1012.